Ocean Engineering 239 (2021) 109844

Contents lists available at ScienceDirect

Ocean Engineering

journal homepage: www.elsevier.com/locate/oceaneng

Extension and improvement of synchronous linear generator based point absorber operation in high wave excitation scenarios

Aitor Saenz-Aguirre [a,*], Alain Ulazia [a], Gabriel Ibarra-Berastegui [b,c], Jon Saenz [d,c]

[a] Energy Engineering Department, University of the Basque Country (UPV/EHU), Otaola 29, 20600 Eibar, Spain
[b] Energy Engineering Department, University of the Basque Country (UPV/EHU), Alda. Urkijo, 48013 Bilbao, Spain
[c] Plentziako Itsas Estazioa (BEGIK), University of Basque Country (UPV/EHU), Areatza Hiribidea 47, 48620 Plentzia, Spain
[d] Department of Physics, University of the Basque Country (UPV/EHU). Sarriena, 48940 Leioa, Spain

ARTICLE INFO

Keywords:
Wave energy
Fluid dynamics
Point absorber
W2W model
High waves
Linear generator
Field weakening

ABSTRACT

The exploitation of marine wave energy resource has led to the design of numerous Wave Energy Converter (WEC) configurations. The power absorption of a WEC is tightly related to its physical properties and the characteristics of the incoming wave front. Additionally, the operational range of a WEC is limited to certain characteristics of the incoming waves. These restrictions are usually related to limitations in the maximum force of the Power Take-off (PTO) system and the safety of the WEC. As a result, the power production of the WEC must be stopped during sea states of high wave elevation. With the objective of improving the operation of a WEC during these sea states, a Field Weakening (FW) control functionality is proposed to be implemented in the control system of a single-body linear in heave oscillating point absorber with a Permanent Magnet Synchronous Linear Generator (PMSLG) based electrical PTO system. The aim of the aforementioned functionality is to attenuate the magnetic flux in the PMSLG during sea states of high wave elevation. The influence of the size of a WEC on the benefits of the proposed FW functionality is also studied. To that end, two point absorbers with different size are analysed with NEMOH and a wave-to-wire (W2W) model of each WEC is developed. This W2W model enables analysis of the performance and power production of the WECs at different sea states of interest. The obtained results show a remarkable improvement of the operation of a WEC with the implementation of the FW strategy during sea states of high excitation, which leads to an extension of its operation and subsequent additional energy/hydrogen generation.

1. Introduction

The design, manufacture and installation of Wave Energy Converters (WECs) has remarkably grown since the early 1980s (Babarit, 2015). The pressure to combat climate change and the necessity to promote alternative renewable energy generation systems have caused the fast development of different WEC technologies, all of them aimed to the exploitation of the wave energy resource (Faizal et al., 2014; Zhao et al., 2020). Many studies have been directed to the estimation and characterization of the huge wave energy resource in various oceanic areas all over the world (Arinaga and Cheung, 2012; Rusu and Onea, 2016).

Among WECs, point absorbers have recently gained in interest due to their reduced dimensions and remarkable power absorption capability in relation to their size (Faizal et al., 2014). These point absorbers, designed to absorb the kinetic energy of the waves in offshore sites, oscillate as a result of the hydrodynamic excitation generated by the waves in the device. Subsequently, this mechanical motion is converted into electrical energy. Regarding their classification (Falcao, 2010), point absorbers are principally categorized with respect to their physical location related to the ocean water level. In this way, floating point absorbers and fully submerged point absorbers are to be differentiated. Comparisonal studies of the performance of both technologies can be found in the literature (Sergiienko et al., 2017). The secondary criterion for the classification of point absorbers is related to the degree of freedom of their motion with respect to the incoming waves. According to this criterion, translational point absorbers (the device oscillates with a linear mechanical motion) and rotational point absorbers (the device oscillates with a rotational mechanical motion) can be distinguished. Finally, point absorbers can also be classified with respect to the number of bodies forming the wave energy exploitation device (Falnes, 1999; Korde, 2003; Wang et al., 2018).

* Corresponding author.
E-mail addresses: aitor.saenz@ehu.eus (A. Saenz-Aguirre), alain.ulazia@ehu.eus (A. Ulazia), gabriel.ibarra@ehu.eus (G. Ibarra-Berastegui), jon.saenz@ehu.eus (J. Saenz).

https://doi.org/10.1016/j.oceaneng.2021.109844
Received 19 March 2021; Received in revised form 18 August 2021; Accepted 11 September 2021
Available online 30 September 2021

List of Abbreviations

WEC	Wave Energy Converter
PMSLG	Permanent Magnet Synchronous Linear Generator
PEC	Power Electronics Converter
PTO	Power Take-Off
FOC	Field Oriented Control
FW	Field Weakening
OWC	Oscillating Water Column
BEM	Boundary Element Method
IRF	Impulse Response Function
W2W	wave-to-wire
UPS	Uninterrupted Power Supply
CCU	Converter Control Unit
ITTC	International Tower Tank Conference

Nomenclature

H_s	Significant wave height
T_p	Peak wave period
$\eta(t)$	Free surface deformations
$z(t)$	Heave displacement of the oscillating body
$\dot{z}(t)$	Heave velocity of the oscillating body
$\ddot{z}(t)$	Heave acceleration of the oscillating body
$f_r(t)$	Radiation force acting on the body
$f_h(t)$	Hydrostatic restoring force acting on the body
$f_e(t)$	Wave excitation force acting on the body
$f_{PTO}(t)$	Force exerted by the PTO system
$f_{PTO\_ref}(t)$	Reference of the force to be exerted by the PTO system
$f_{em}(t)$	Electromagnetic force in the stator
$\theta_s(t)$	Electrical angle in the stator of the PMSLG
$w_s(t)$	Electrical frequency in the stator of the PMSLG
$v_{sd}(t)$	Stator voltage in the synchronous d axis
$v_{sq}(t)$	Stator voltage in the synchronous q axis
$i_{sd}(t)$	Stator current in the synchronous d axis
$i_{sq}(t)$	Stator current in the synchronous q axis
$I_{s\_abc}(t)$	Three-phase stator current
$V_{s\_abc}(t)$	Three-phase stator voltage
$P_s(t)$	Generated stator power

To the present day, the most widely studied wave energy absorption devices are the single-body in heave oscillating linear point absorbers. In order to understand, and mathematically characterize, the interaction between the waves and these point absorbers, the hydrodynamics of in heave oscillating bodies of different forms (flat plate Bezunartea-Barrio et al., 2020, cylinder Gaeta et al., 2020 and cone Rusch et al., 2020) have been studied in detail in the literature. Moreover, the effect of increasing the size of the floating body has also been object of study (Bezunartea-Barrio et al., 2020). According to the results of this latter analysis, the radiation damping of the point absorber is heavily influenced by the frequency of the incoming wave front and the size of the device. Hence, it is concluded that the performance of the WEC is tightly related to its geometry. Additionally, WEC design, selection and placing procedures based on optimization problems can also be found in the literature (Piscopo et al., 2018; Vantorre et al., 2004; Child and Venugopal, 2010; Borgarino et al., 2012). The aim of such optimization procedures is the selection of the optimal WEC device for a predefined application and considering the techno-economic constraints (Garcia-Teruel et al., 2020; Sirigu et al., 2020).

Prototypes of in heave oscillating linear point absorbers have also been installed and tested in real wave conditions. The first prototype, called Power Buoy (Edwards et al., 2014), has a rated power of 3 kW and is formed by a floating body and a damping heave plate moored to the ocean floor. While the damping plate is designed to attenuate the vertical displacements of the device, the floating body is free to oscillate in heave. This linear motion is later converted into rotatory motion and electricity is generated by means of a rotating electrical generator. Another prototype, the Uppsala University point absorber (Danielsson, 2006), has a rated power of 10 kW and consists of a floating cylindrical buoy, connected to a gravity-based foundation. The electricity is generated with a Permanent Magnet Synchronous Linear Generator (PMSLG). Finally, the L10 prototype (Ruehl, 2011), with a diameter of 3.5 m and a rated power of 10 kW, was designed by the University of Oregon and successfully tested in Newport, Oregon, in September 2008. All these prototypes have contributed to the increase of the industrial maturity of the technology.

An important aspect to consider related to the operation of point absorbers is the selection and design of the Power Take-Off (PTO) system. In WECs, a double objective is pursued with the PTO system: conversion of the mechanical oscillation into electrical power and regulation of the point absorber motion, to the end of maximizing its power absorption. In case of linear point absorbers, the design and application of hydraulic PTOs (Cargo et al., 2012; Hansen et al., 2013; António, 2008) and electrical PTOs (Prudell et al., 2010; Polinder et al., 2004; Ivanova et al., 2005) have been extensively described in the literature. In both cases, the force the PTO system exerts to the point absorber is aimed to influence its motion and maximize the power absorption. Therefore, the design of many control strategies (implemented in a generic PTO system) have been proposed in the literature: Latching control (Babarit and Clément, 2006), velocity tracking based model predictive control (Cretel et al., 2011), proportional control (Coe et al., 2020) and pseudo-spectral control (Bacelli and Coe, 2020).

In application to in heave oscillating linear point absorbers, the employment of electrical PTOs results easier than hydraulic PTOs, since no intermediate conversion of the linear mechanical motion into rotatory is required. In fact, the use of a PMSLG enables direct conversion of the linear mechanical motion into electrical power. The design procedure of a synchronous linear generator for wave energy generation is presented in the work of Calado et al. (2012). In such generators, the magnetic flux of the rotor is produced by the permanent magnets and the magnetic flux, electrical current and power in the stator are generated as a result of the motion of the rotor and its magnets.

The employment of a PMSLG as the PTO system of a WEC requires the implementation of a control logic for the electrical generator, aimed to ensure the adequate tracking of the set point generated by the WEC controller and the safety of the generator. The basic control strategy applied to electrical machines is the Field Oriented Control (FOC), which has been widely studied in the literature (Mayo et al., 2020; Wang et al., 2015; Ma et al., 2001). The basic principle of the FOC strategy is the decoupling of the stator current in the synchronous *dq* axes and their independent control. Additionally, some features can be introduced in order to improve the performance of such controllers, one of them being the Field Weakening (FW) strategy, which allows attenuation of the statoric magnetic field in case of high magnetization. An overview of various FW strategies is presented in the work of Lu and Kar (2010). According to this review, FW strategies can be divided into two main groups: improved magnetic design of the electrical drive (Xu et al., 1995) and control functionalities based on power electronics (Tursini et al., 2009). Recent examples of implementation of a FW functionality for control purposes of electrical generators in wave energy applications (Oscillating Water Column (OWC) Ramirez

et al., 2019, WEC Ammar et al., 2017; Sullivan and Lightbody, 2016) can been found in the literature. All of them stress the importance of such a strategy to avoid damages and improve operation of the systems during situations of high speed. In the present work, the analysis has been expanded and the potential benefits (in terms of additional energy/hydrogen generation at real oceanic locations) of extending the operation of a WEC, by means of a FW strategy, have been computed. Note that hydrogen generation will be calculated out of the produced energy (Serna and Tadeo, 2014), and will be used as an indicator of the production of the WECs, as wave resource measurement data used in the validation procedure have been obtained from far offshore locations.

Regarding the operation of linear point absorbers, it is usually limited to a predefined range, described with the significant wave height H_s and peak wave period T_p of the incoming wave front (Rusu and Onea, 2018). For waves with peak periods T_p outside the range, or significant wave heights H_s below the cut-in value, the excitation induced in the point absorber is not high enough to sustent its operation. On the contrary, for significant wave heights H_s above the cut-out value, the operation is restricted to preserve the integrity of the device. For instance, as a result of high waves, the operation of the WEC could be worsened due to the reduced performance of the PTO system, which faces a maximum force limitation (Coe et al., 2020). In higher wave conditions, excessive mechanical loads could be induced in the point absorber (Neary et al., 2020) and its operation stopped for safety reasons. An extreme wave conditions analysis prior to installation of a WEC must be performed in order to guarantee the integrity of the device under extreme environmental conditions (Neary et al., 2020).

In this paper, a FW functionality, implemented in the FOC control system of the PMSLG, is presented to improve and extend the operation of in heave oscillating linear point absorbers in scenarios of high wave excitation. In those cases, the velocity of the floating body increases as a result of the high excitation of the waves, and, consequently, the magnetization of the stator of the PMSLG is remarkably incremented. On account of this high statoric magnetic field and the voltage limitations of the actuator, the regulation performance of the PTO system is remarkably worsened. Thus, the demagnetization of the magnetic field, by means of a FW functionality, could help improve the performance of the PTO system and, therefore, extend the operation and energy/hydrogen generation of a WEC.

Furthermore, the relation between the size of a WEC and the potential benefits of the proposed FW strategy is also studied in this paper. To that end, the proposed strategy is applied to two point absorbers of different form and size. In both cases, the hydrodynamic parameters of the floating body are calculated with the Boundary Element Method (BEM) code NEMOH (NREL NWTC, 2020; Babarit and Delhommeau, 2015). Subsequently, the equations of the motion of the single-body point absorber (including the hydrodynamic parameters), a model of a PMSLG and the control strategies are implemented in Matlab/Simulink. By combining all of them, a wave-to-wire (W2W) model (Penalba and Ringwood, 2019, 2020) of the WEC is obtained, in which the temporal wave elevation data is the only input and any variable associated to the performance of the WEC can be analysed, with special mention to the generated power. The irregular wave elevation data for the simulation based validation of the FW functionality are generated with the module Hydrodyn (Jonkman et al., 2015). Finally, the additional energy and hydrogen production of a WEC (due to extension of its operation with the proposed FW functionality) in four far offshore locations and one nearshore location have been computed using real wave resource data from the Atlantic ocean and the Biscay coast, respectively. These data have been obtained using *ERA5* (Hersbach et al., 2020), a widely employed tool for meteorological studies all around the world.

This paper is structured as follows: In Section 2 the design of the W2W model is described, including the wave data generation, the hydrodynamics and motion modelling of the point absorber, the PTO system and the control strategy. In Sections 3 and 4, the obtained results and the discussion are presented, respectively. Finally, the conclusions of the conducted analysis are explained in Section 5.

2. Wave energy converter: W2W model

2.1. Wave data

The operation and power production of a WEC are, at first instance, defined by the wave resource at the installation site of the device. In order to ensure its correct performance in advance, the operation of a WEC at various sea states can be analysed in simulation. In this case, the wave elevation data for the design and simulation of the proposed W2W model have been obtained using the module Hydrodyn (Jonkman et al., 2015), which is part of the aeroelastic code FAST v8 (LHEEA Centrale Nantes, 2019). The aforementioned Hydrodyn module enables creation of wave elevation data with high temporal resolution and defined by various physical and meteorological parameters, the most important being the significant wave height H_s and the peak wave period T_p. Additionally, the wave data can be generated to be spread in different directions and according to diverse ocean wave spectra.

The wave elevation data generated for the present analysis are based on the JONSWAP spectrum (Hasselmann et al., 1973; Pierson and Moskowitz, 1964), which describes the concept of developing sea states and is widely employed in oceanography for extreme event analysis. The peak enhancement factor for the aforementioned spectrum is calculated following the methodology in IEC 61400-3 Annex B, i.e. based on the peak wave period T_p and the significant wave height H_s. The time step for the output data has been set to 0.125 s (more than ten times the lowest period expected for the waves, in order to ensure that all frequencies get adequately modelled). Finally, the significant wave height H_s and the peak wave period T_p will be modified to characterize various wave scenarios. The obtained wave elevation data are directly applied to the W2W model as an input in format of temporal series.

2.2. Hydrodynamics and motion of the point absorber

The WECs considered in this analysis are based on two different existing configurations of a single-body linear point absorber. The first point absorber, from now on addressed as WaveBot, is inspired in the geometry of the commercial WaveBot device (Coe et al., 2016). The second point absorber, addressed as Flat, is based on the flat geometry of the Uppsala floating device (Danielsson, 2006). In both cases, the motion of the oscillating body is restricted to an in heave linear oscillation, which is to be converted into electrical energy by means of a PTO system. Linear in heave oscillating point absorbers are designed either to be moored to the ocean floor or to a submerged platform (Brekken, 2011), which is usually the preferable solution for far offshore energy production farms. In this case, the functional design procedure of the point absorber is accomplished by considering an adequately moored device. Potential constraints arising from the design of the mooring system could be applied in a posterior procedure.

The main physical characteristics of both point absorber devices designed for the present analysis are listed in Table 1. As it is to be noticed, the Flat point absorber has a bigger size and mass than the WaveBot device. The objective of comparing both floating bodies is to relate the benefits of the proposed FW control functionality to the size of the point absorber and, thus, their different hydrodynamic properties.

The computation of the hydrodynamic parameters corresponding to both point absorbers has been performed with the open source BEM code NEMOH (NREL NWTC, 2020; Babarit and Delhommeau, 2015). By means of this code, the radiated and diffracted velocity fields are computed and the frequency-dependent radiation damping, radiation added mass and excitation coefficient of both floating bodies are calculated. As a result, the performance of the floating body under interaction with the waves gets fully characterized. The number of panels defined for the mesh and posterior hydrodynamic analysis of each point absorber has been defined as 200 and 400, respectively. The mesh for both point absorbers are shown in Figs. 1a and 1b.

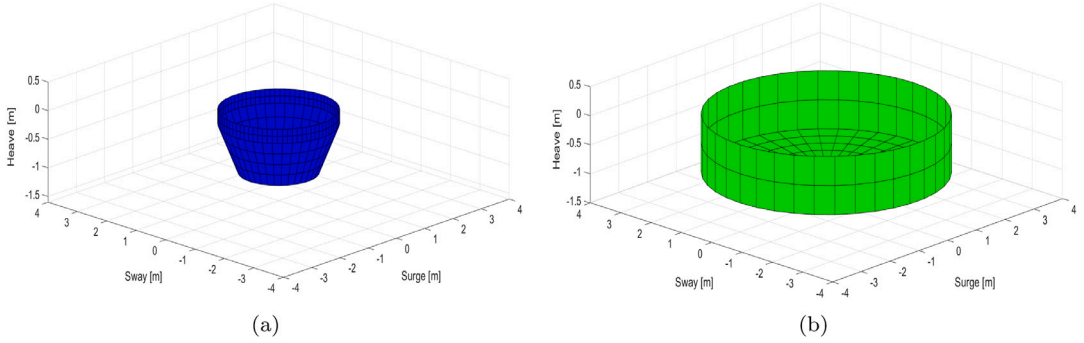

Fig. 1. Mesh for the hydrodynamic analysis with NEMOH (a) WaveBot point absorber (b) Flat point absorber.

Table 1
Main physical characteristics of the designed point absorber devices.

Physical characteristics of the point absorbers				
			WaveBot	Flat
Description	Parameter	Unit	Value	
Height of the floating body	H	m	1.1	1
Width of the floating body	D	m	3	6
Mass of the floating body	M	kg	6117	28 849

The dynamics of in heave oscillating linear point absorbers have been extensively studied in the literature (António, 2008; Babarit and Clément, 2006). The time-domain expression for the linear modelling of single-body floating devices is shown in Eq. (1), which is based on the notorious Cummins equation (Cummins, 1962).

$$M\ddot{z}(t) = f_e(t) - f_r(t) - f_h(t) - f_{PTO}(t) \tag{1}$$

The radiation force (Faedo et al., 2018), as shown in Eq. (2), is modelled as the sum of the added mass at infinite frequency and the convolution integral of the causal radiation Impulse Response Function (IRF) of the floating body.

$$f_r(t) = \mu_\infty \ddot{z}(t) + \int_0^t k_r(t-\tau)\dot{z}(\tau)\,d\tau \tag{2}$$

where μ_∞ is the radiation added mass at infinite frequency and k_r represents the radiation IRF.

The hydrostatic force is calculated with the hydrostatic stiffness (k_h) of the floating body, $f_h(t) = k_h z(t)$, and the excitation force is modelled as $f_e(t) = Fe \cdot \eta(t)$, with the normalized excitation force on the body (Fe) previously calculated using linearized potential flow theory with NEMOH (Genest and Ringwood, 2016).

Note that at this stage the non-linearity associated to the Froude–Krylov force, see Giorgi et al. (2016, 2020), has not been considered in the modelling of the motion. Nonetheless, in light of its relevance in the motion of axisymmetric floating bodies under controller conditions, its introduction will be studied for future analyses.

2.3. PTO system

The PTO system proposed in this paper for the electrical power generation, see Fig. 2, is formed by the combination of a PMSLG and a Power Electronics Converter (PEC), which is used to have control over the electromagnetic force generated by the linear generator. As the power source of the PEC, an Uninterrupted Power Supply (UPS) is considered, which could correspond either to the electrical grid in nearshore applications or to a hydrogen based fuel cell in far offshore applications.

The double purpose of the PTO system is to convert the mechanical power of the oscillating body into electrical energy and actuate on the point absorber with the objective of maximizing its power absorption (Falcao, 2010). The main advantage of using a PMSLG as PTO system with in heave linear oscillating devices is that the mechanical power of the point absorber can be directly transformed into electrical energy. Other PTO techniques, such as an hydraulic system, would require a previous transformation of the linear oscillation into rotatory motion, which introduces extra elements and complexity to the system (Kassem et al., 2015). The principal parameters of the proposed PMSLG are listed in Table 2.

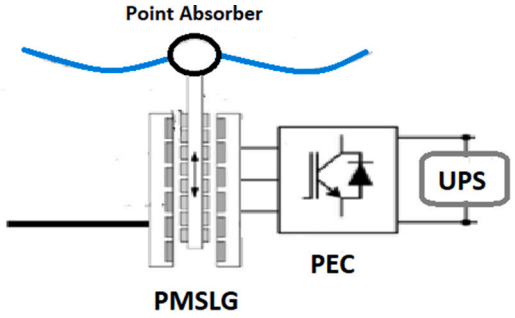

Fig. 2. Schematic diagram of the PTO system for the electrical power generation.

Table 2
Principal parameters of the PMSLG considered in the electrical PTO system.

Permanent magnet synchronous linear generator			
Description	Parameter	Unit	Value
Rated RMS stator voltage	V_{s_rated}	V	220
Resistance of the stator	R_s	Ω	$75 \cdot 10^{-3}$
Inductance of the stator	L_s	H	$3020 \cdot 10^{-5}$
Pole pairs	p	–	2
Magnetic flux of the poles	σ	Vs	25
Length of the stator	L	m	3

In case of a PMSLG, the force exerted by the PTO system $f_{PTO}(t)$ corresponds to the electromagnetic force $f_{em}(t)$ generated in the stator of the electrical machine. Consequently, the force the PTO system exerts in the floating body can be controlled by regulation of this electromagnetic force. According to the FOC theory (Mayo et al., 2020; Sullivan and Lightbody, 2016; Ammar et al., 2017), the operation of an electrical generator can be controlled by regulation of its statoric electrical current in the synchronous dq axes. The transformation of sinusoidal 3-phase signals into the synchronous dq axes is achieved by means of the Park transformation (Park, 1929). Additionally, according to the same FOC theory, if the control system aligns the rotor flux of the generator with one of the synchronous dq axes, by means of an adequate phase definition in the current injection, the electromagnetic force induced in the stator of the generator is directly proportional to

the current in the opposite axis, as shown in Eq. (3).

$$f_{PTO}(t) = f_{em}(t) = \frac{3\pi p \sigma i_{sq}(t)}{L} \tag{3}$$

where $f_{em}(t)$ is the electromagnetic force in the stator of the PMLSG and $i_{sq}(t)$ is the stator current in the synchronous q axis.

The expression of the electrical angle $\theta_s(t)$ used for the alignment with the synchronous axes is shown in Eq. (4). Likewise, the mathematical expressions corresponding to the electrical voltage in the stator of the linear generator in the synchronous dq axes are shown in Eq. (6) and (7).

$$\theta_s(t) = \frac{2\pi p z(t)}{L} \tag{4}$$

$$w_s(t) = \frac{d\theta_s(t)}{dt} \tag{5}$$

$$v_{sd}(t) = R_s i_{sd}(t) + L_s \frac{di_{sd}(t)}{dt} - L_s w_s(t) i_{sq}(t) \tag{6}$$

$$v_{sq}(t) = R_s i_{sq}(t) + L_s \frac{di_{sq}(t)}{dt} + L_s w_s(t) i_{sd}(t) + w_s(t)\sigma \tag{7}$$

where $z(t)$ is the in heave displacement of the floating body, $w_s(t)$ is the frequency of the electrical variables in the stator of the PMSLG and $i_{sd}(t)$, $i_{sq}(t)$, $v_{sd}(t)$ and $v_{sq}(t)$ are the stator current and voltages in the synchronous dq axes.

As a result, it is demonstrated that the heave velocity of the oscillating body $\dot{z}(t)$ (Eq. (5)) has a direct impact on the stator currents (Eqs. (6) and (7)) and, hence, on the force exerted by the PTO system $f_{PTO}(t)$ (Eq. (3)). Likewise, it is shown that the force $f_{PTO}(t)$ and, ultimately, the motion of the oscillating body can be influenced by actuating on the stator voltage $v_{sd}(t)$ and $v_{sq}(t)$. To that end, the power electronics converter and the associated control strategy are employed. The control strategy proposed in this paper is based on the same principle as the original FOC strategy and presents, thus, a double control objective: On the one hand, by controlling the stator current in the synchronous q axis, the force $f_{PTO}(t)$ induced in the linear oscillating body can be regulated. On the other hand, by controlling the stator current in the synchronous d axis, a FW functionality can be implemented in order to reduce the magnetic flux in the stator in cases of high wave excitation, see Ramirez et al. (2019) for more detail. During normal operation of the electrical drive, without FW, the regulation of the stator current in the synchronous d axis would serve to control the reactive power generation of the system, in case any grid support requirements should be met.

2.4. PTO control strategy

The control strategy of the PTO system is formed by two regulation loops: the WEC controller (it is the outer controller, in open loop form, which calculates the force $f_{PTO\_ref}(t)$ the PTO system must exert in the floating device) and the PMSLG controller (it is the inner controller, in closed loop form, which receives the reference of the force $f_{PTO\_ref}(t)$ from the outer controller and ensures its adequate tracking by regulation of the electrical currents in the linear generator). Thus, the implementation of both controllers in a joint simulation is important to detect possible interactions between both regulators and adequately treat limitations that could affect either controller.

Regarding the WEC controller, many strategies have been proposed in the literature for this purpose (Babarit and Clément, 2006; Cretel et al., 2011; Coe et al., 2020; Bacelli and Coe, 2020). The complex-conjugate control strategy (Falcão, 2010), valid for regular wave conditions only, provides the mathematically optimal force $f_{PTO}(t)$ the PTO system should apply in the oscillating body in order to maximize its power absorption. The practical application of this optimal force is complicated mainly due to two reasons: the variability of the frequency of the incident waves and the power limitations of the PTO system (García-Violini et al., 2020). A review of simple controllers applicable in real scenarios is presented in the work of García-Violini et al. (2020). In this paper, a simple proportional damping controller (Coe et al., 2020) is proposed as the WEC controller, see Eq. (8).

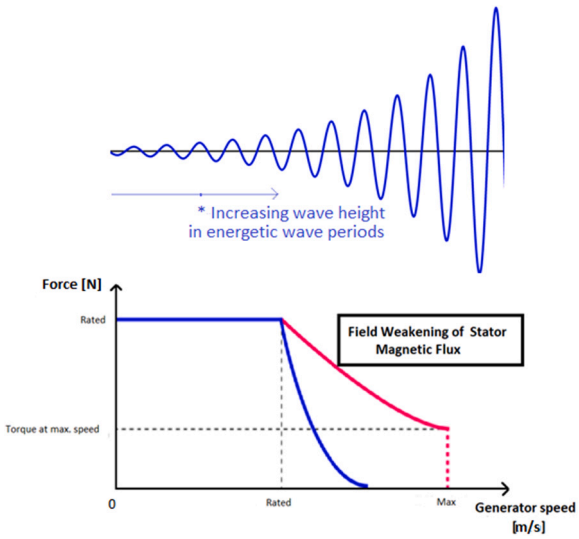

Fig. 3. Theoretical diagram of the actuation of the FW functionality applied to a wave energy driven electrical machine: without FW (blue), with FW (pink). (For interpretation of the references to colour in this figure legend, the reader is referred to the web version of this article.)

$$f_{PTO\_ref}(t) = B_{PTO}\dot{z}(t) \tag{8}$$

where $\dot{z}(t)$ is the in heave velocity of the floating body.

Regarding the PMSLG controller, as previously introduced, a FOC strategy is proposed in this paper for the tracking of the reference PTO force $f_{PTO\_ref}(t)$ calculated by the WEC outer regulator. In FOC control, as shown in Eq. (3), the tracking of the reference PTO force is ensured by means of the closed loop regulation of the stator current in the synchronous q axis. Additionally, in order to improve the performance of the FOC control system in scenarios of high wave excitation, a FW control functionality has been added in this paper. The goal of the FW strategy is to attenuate the statoric magnetic flux in cases of high velocity of the rotor. As a result, an improved performance of the whole system at high speeds is expected, as well as the possibility to extend the operational range of the WEC.

As shown in Fig. 3, the FW functionality allows operation of the electrical generator at high speeds. This is achieved by means of attenuating its statoric magnetic field (Ramirez et al., 2019). Since the FW is accomplished by regulation of the stator current in the synchronous d axis, see Eq. (7), either the rotor torque must be reduced (see pink line in Fig. 3) or it must be accounted for a greater current flow through the electrical system. Applied to the operation of WECs, since the high speed situations are prone to happen in high wave elevation scenarios, the FW functionality could help improve and extend the operation of the WECs to higher wave height scenarios (Ammar et al., 2017; Sullivan and Lightbody, 2016)). In this case, the set point of the d axis stator current has been made adaptive with respect to the linear velocity of the rotor, using an interpolation table. The current design makes the electrical system to be unable to effectively ensure tracking of the reference force $f_{PTO\_ref}(t)$ for heave velocities greater than 3.5 m/s. Consequently, at low velocities, no d axis stator current is injected. However, by increasing the heave velocity, the set point i_{sd_ref} must be incremented.

The tuning of the control parameters is shown in Table 3. For the proportional PTO controller, the definition of the B_{PTO} gain value is based on the premise that the reference PTO force $f_{PTO\_ref(t)}$ does not reach saturation until approximately the original wave height cut-out value of the system, in this case 6 m. For the tuning of the controllers

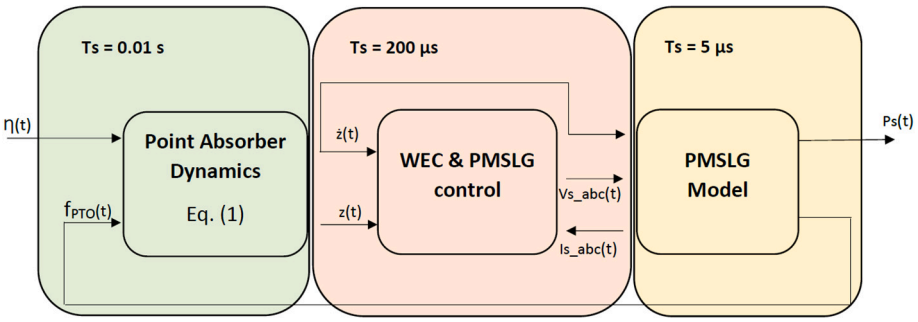

Fig. 4. Schematic diagram of the W2W model developed in Matlab/Simulink.

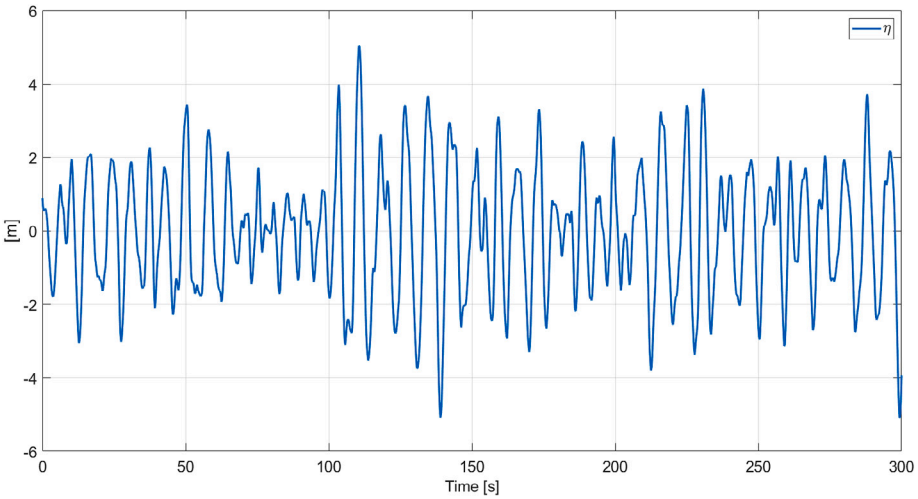

Fig. 5. Wave elevation data generated with Hydrodyn module.

Table 3
Definition of the WEC (outer loop) and PMSLG (inner loop) controller parameters.

Control system parameters			
Description	Parameter	Unit	Value
Proportional PTO coefficient	B_{PTO}	Ns/m	10 000
Maximum PTO system force	f_{PTO_max}	kN	30
Proportional gain i_{sd} control loop	$Kp_{\_i_{sd}}$	V/A	50
Integral gain i_{sd} control loop	$Ki_{\_i_{sd}}$	V/A	10
Proportional gain i_{sq} control loop	$Kp_{\_i_{sq}}$	V/A	50
Integral gain i_{sq} control loop	$Ki_{\_i_{sq}}$	V/A	10
FW interpolation table (i_{sd_ref} vs. $\dot{z}$)	i_{sd_ref}	m/s A	[0,3,4,7,10] [0,0,−400,−550,−550]

related to the FOC control (i_{sd} and i_{sq} control loops), the locations of the closed loop poles as well as the phase margin and bandwidth have been considered to ensure a correct response of the system. Finally, the d axis stator current set point corresponding to the FW functionality has been defined in form of an interpolation table.

The model of the point absorber, the PMSLG model and the control system are all combined and implemented in Matlab/Simulink to form the W2W model, see Fig. 4. As previously introduced, the performance and power production of a WEC under different wave resource scenarios can be studied using this W2W model. The execution time step of the point absorber model is set to 0.01 s, the execution time step of the PMSLG model is set to 5 µs and the execution time step of the control system is set to 200 µs. The selection of the time steps is the result of a compromise between the computational burden, on the one hand, and the frequencies of the signals that are modelled and the assurance of stability of the model, on the other.

The interaction between the different elements of the W2W model can be observed in Fig. 4. The input of the model is the instantaneous wave elevation data, see Section 2.1. The hydrodynamic parameters of the point absorber (calculated following the methodology presented in Section 2.2) are implemented in the block named "Point Absorber Dynamics", which corresponds to the equation of motion of the point absorber. The model of the PMSLG, implemented in the block named "PMSLG Model" and described in Section 2.3, receives the actuation of the control system ("WEC & PMSLG control" block) and generates the electromagnetic force (or f_{PTO}) that is applied to the point absorber and influences its motion. Finally, the generated power can be measured at the stator windings of the PMSLG.

3. Results

3.1. Wave data

Instantaneous wave elevation data corresponding to a sea state defined by a significant wave height of $H_s = 8$ m and a wave peak period of $T_p = 8$ s have been generated for the validation of the proposed FW functionality. The data generation has been accomplished with the module Hydrodyn and following the methodology presented in Section 2.1. Since no statistical properties are to be extracted from the results in this simulation, solely graphical representation and conceptual validation, the duration of the simulation has been defined as 300 s, as shown in Fig. 5.

The generated wave elevation data contains sufficient scenarios for the conceptual validation of the FW strategy, as it presents intervals with low wave elevation (during which the floating body should operate normally, as the heave velocity threshold to activate the FW

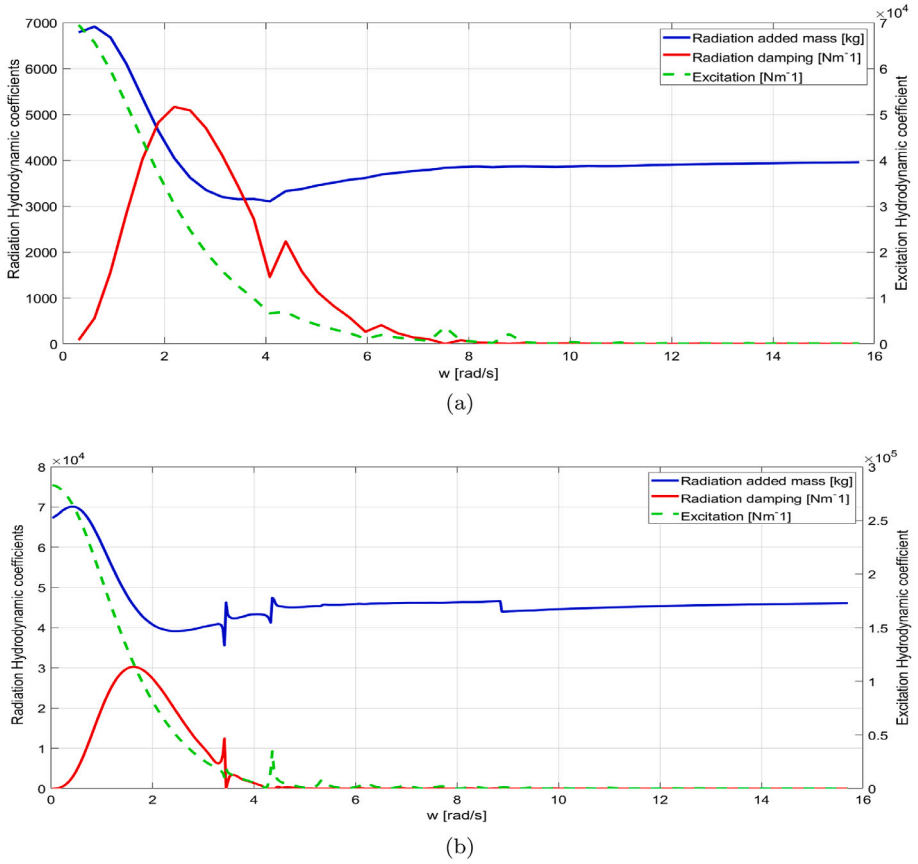

Fig. 6. Hydrodynamic parameters calculated with NEMOH (a) WaveBot point absorber (b) Flat point absorber.

functionality should not be reached) and it also presents intervals with high wave elevation (during which the floating body will not be able operate normally without the FW functionality, since the heave velocity threshold that causes the high magnetization of the stator will be reached, and the electrical system will be unable to effectively regulate the electromagnetic force). In order to analyse the performance and power production of the WECs during this sea state, the wave elevation data array is supplied to the W2W model, presented in Section 2.

3.2. Hydrodynamics of point absorber

The interaction of a floating body with the incoming wave front, and in consequence its motion, are essentially defined by the inertial forces that arise from the potential flow theory. In this case, as introduced in Section 2.2, the hydrodynamic equations corresponding to both point absorber geometries have been solved with the BEM code NEMOH and the added mass [kg], the radiation damping [N/(m/s)] and the excitation coefficient [N/m] with respect to the frequency of the incoming wave front have been calculated and represented in Figs. 6a and 6b, respectively.

The results are in concordance with similar studies in the literature (Isaacson et al., 1990; Gaeta et al., 2020) and, as expected, the hydrodynamic analysis shows a remarkable correlation between the geometry of the point absorber and the frequential evolution of the inertial forces acting on it. Regarding the added mass, it is incremented by increasing the cross-sectional area of the point absorber. Regarding the radiation damping, the increase of the size of the WEC shows a considerable effect on its frequential evolution, shifting the value of the maximum radiation damping to lower wave frequency values. In absolute terms, the value of the radiation damping is increased by incrementing its size. Finally, in line with the radiation damping, the excitation coefficient shows a tendency to be reduced for higher wave frequencies when the size of the WEC is incremented. In absolute terms, the value of the excitation force is also increased by incrementing its size.

The variation of the hydrodynamic forces acting on the point absorber has a direct impact on the motion, and thus, power capture, of the WEC. Hence, by applying the hydrodynamic parameters in the W2W model, the joint performance of the point absorber and the PTO system during different sea states of interest can be analysed in detail.

3.3. Point absorber operation improvement

In this subsection, the operation and power production of both WECs during the sea state shown in Section 3.1 is presented. To that end, the instantaneous wave elevation data is applied to the corresponding W2W model and an analysis of the motion of the point absorber, the electrical performance of the PTO system and the power generation of the WEC is carried out. Moreover, the effect of implementing the FW strategy is also studied.

3.3.1. WaveBot point absorber

The simulation results of the W2W model corresponding to the WaveBot point absorber and without implementation of the FW functionality are shown in Fig. 7. The wave elevation $\eta(t)$ and the in heave motion of the point absorber $z(t)$ are represented in the upper plot. The upper middle plot shows the motion velocity of the point absorber $\dot{z}(t)$. The middle plot presents the reference PTO force $f_{PTO\_ref}(t)$ and the corresponding instantaneous force $f_{PTO}(t)$ exerted by the PTO system in the floating device. The lower middle plot shows the instantaneous three-phase electrical current through the stator windings of the electrical generator $I_{s\_abc}(t)$. Finally, the lower plot represents the instantaneous power generated in the stator of the electrical generator $P_s(t)$.

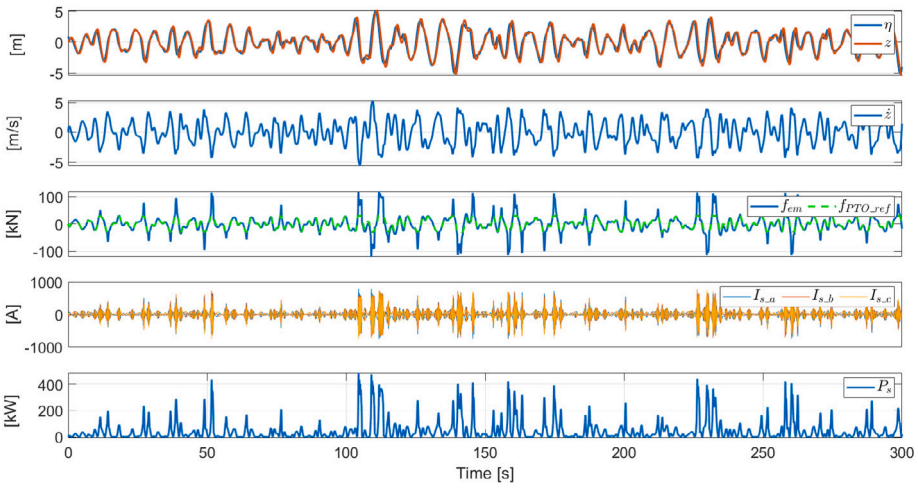

Fig. 7. Temporal performance of the WaveBot WEC with no FW.

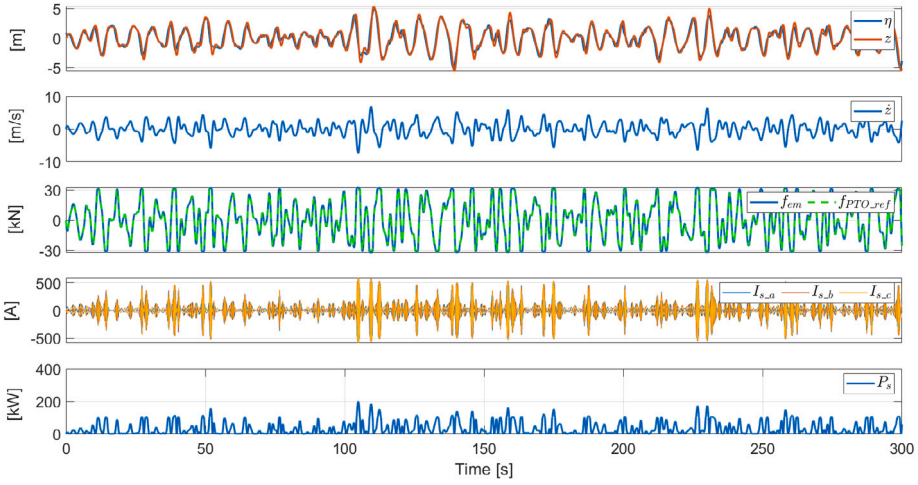

Fig. 8. Temporal performance of the WaveBot WEC with FW.

The obtained results support the expected premises, since an inadequate operation of the PTO system is observed when the instantaneous wave elevation increases. While the wave elevation is low, the limited excitation of the waves on the floating body causes neither abrupt motions of the floating body nor high heave velocities, which enables an adequate operation of the PTO system. Nevertheless, as a result of the excitation exerted by high waves to the point absorber, the motion velocity of the floating body $\dot{z}(t)$ becomes higher, and, consequently, the magnetic flux in the stator of the PMSLG is incremented, see Eq. (7). Subsequently, on account of the voltage limitation of the electrical system, its control capability is lost and the stator currents $I_{s\_abc}(t)$, the electromagnetic force $f_{em}(t)$ and the stator power $P_s(t)$ grow uncontrollably. During this scenario, the tracking of the reference PTO force $f_{PTO\_ref}(t)$ is impossible and the WEC should be stopped due to its safety not being guaranteed.

The application of the FW strategy proposed in this paper is aimed to solve the problem identified in Fig. 7. In order to validate the benefits associated to the implementation of the FW strategy, the simulation results of the WaveBot point absorber with implementation of the FW strategy are shown in Fig. 8. The order of the depicted variables has been maintained with respect to the previous figure in this Subsection.

The simulation results depicted in Fig. 8 show a significantly improved operation of the PTO system with high wave elevation (and subsequent high excitation of the point absorber) with the application of the FW functionality. In fact, in comparison to the same scenario in Fig. 7, the results in Fig. 8 present an adequate tracking of the reference PTO force $f_{PTO\_ref}(t)$ during the whole simulation. By reason of the FW functionality, in cases of high excitation of the point absorber, stator current in the synchronous d axis is injected in a controlled way and the magnetic flux in the stator of the PMSLG is attenuated. As a result, the voltage limitation of the electrical system is not reached and the operation of the WEC is kept under control.

By comparing simulation results in Figs. 7 and 8, an increase of the heave velocity of the point absorber $\dot{z}(t)$ after implementation of the FW functionality can be observed during certain periods. It must be noted that in the results shown in Fig. 7, the application of extremely high $f_{em}(t)$ forces is observable, far beyond the maximum capability of the electrical system. This behaviour is not realistic, only numerical, and evidences the impossibility of the electrical system to operate in such conditions. With the application of this unreal and high force, the heave velocity $\dot{z}(t)$ is kept low. In contrast, in the results shown in Fig. 8, the heave velocity $\dot{z}(t)$, grows bigger, which responds to the application of a lower but realistic $f_{em}(t)$ force, which is saturated to the maximum capability of the electrical system.

Finally, it should be noted that, as a result of the FW implementation and on account of the necessity to attenuate the statoric magnetic flux, a high stator current in the synchronous d axis could be injected during some instants. Hence, the power flow could be reverted, which would result in power consumption. The application of the FW strategy must be subject to a double condition: On the one hand, its implementation

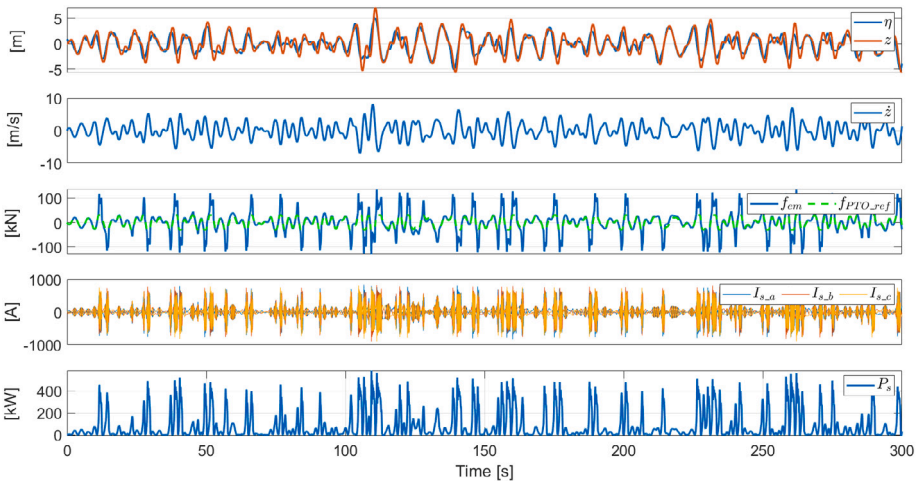

Fig. 9. Temporal performance of the Flat WEC with no FW and during the sea states of interest.

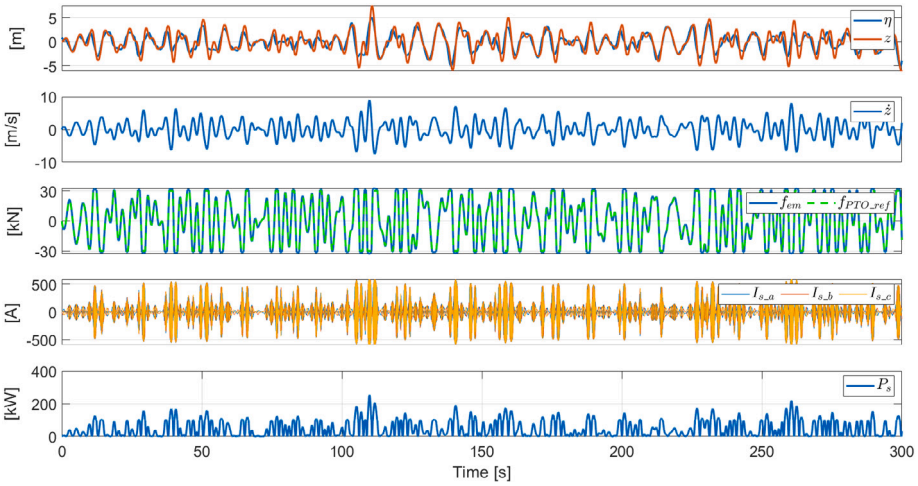

Fig. 10. Temporal performance of the Flat WEC with FW and during the sea states of interest.

will only be legit if the mean power generation exceeds the mean power consumption caused by the FW functionality. On the other hand, the necessity to inject stator current in order to attenuate the magnetic flux must be taken into consideration when designing the electrical system and its maximal electrical current values.

3.3.2. Flat point absorber

The simulation results of the Flat point absorber without implementation of the FW strategy are shown in Fig. 9. The order of the depicted variables has been maintained following the example of the figures in the previous Subsection.

The results obtained in Fig. 9 validate again the expected assumptions, as the excitation of the high waves on the floating body cause high heave velocities $\dot{z}(t)$ and performance loss of the PTO system. The fast motions of the floating body cause an increment of the magnetic flux on the stator of the PMSLG and, in consequence, the voltage capability of the PTO system is exceeded and the control over the reference PTO force $f_{PTO\_ref}(t)$ is lost. Subsequently, the motion of the WEC is uncontrolled and the integrity of the PTO system, in this case the PMLSG, is compromised due to overcurrents.

The simulation results of the Flat point absorber with implementation of the FW strategy are shown in Fig. 10. The order of the depicted variables has been maintained with respect to the previous figure in this Subsection.

The obtained results show that, as expected, the tracking of the reference PTO force $f_{PTO\_ref}(t)$ is considerably improved with the application of the FW strategy. Moreover, the overcurrents that may endanger the safety of the electrical system have been removed and substituted by a controlled current injection aimed to reduce the magnetization of the stator. Hence, the safety of the WEC is guaranteed and its operation sustained.

In comparison to the application of the FW strategy in the WaveBot point absorber, see Fig. 8, it is to be noted that with the larger Flat point absorber the electrical current injection for the demagnetization of the stator has been increased. As a consequence of the bigger mass of the device, the recovery from the high excitation period is worsened (see oscillations in heave velocity $\dot{z}(t)$), and the actuation of the FW functionality has been necessary on more occasions.

3.4. Extension of operation and power matrix

The effect of implementing the proposed FW strategy in both WECs, in terms of operational range extension, is analysed in this subsection. As it has been demonstrated in Section 3.3, the application of the FW strategy is based on the controlled current injection in order to attenuate the magnetic flux in the stator of the PMSLG, and, thus ensure the adequate tracking of the reference PTO force and the safety of the WEC. As a result, the operation of the WEC can be extended to higher (or additional) significant wave height H_s values, see first column in Table 4.

However, the injection of additional current due to the FW strategy is linked to an increase of the dimensions and capability of the electrical

Table 4
Extension of the power matrix [kW] by application of the FW functionality (a) WaveBot point absorber (b) Flat point absorber.

(*a*)

		T_p [s]						
		2	4	6	8	10	12	14
H_s [m]	8.5	–	–	62.82	42.02	29.02	22.48	19.29
	8	–	–	57.45	38.48	26.37	20.86	17.77
	7.5	–	–	52.08	34.96	24.02	19.22	15.92
	7	–	–	46.96	31.44	22.03	17.57	13.97
	6.5	–	–	42	27.91	20	15.92	12.11

(*b*)

		T_p [s]						
		2	4	6	8	10	12	14
H_s [m]	8.5	–	–	78.44	55.41	38.8	31.32	27.13
	8	–	–	72.09	51.04	35.53	29.47	25.37
	7.5	–	–	66.03	46.7	32.76	27.57	23.05
	7	–	–	60.1	42.43	30.6	25.63	20.48
	6.5	–	–	54.35	38.18	28.37	23.64	17.94

system, which results in a bigger economical cost. In this case, in order to relate the benefits of the FW strategy to the overdimensioning of the electrical system, two maximum electrical current values have been defined and the operation of the WECs with the FW functionality has been extended until the restriction of maximum current capability has been met. The extensions of the power matrix (in [kW]) for both WEC devices are shown in Table 4, respectively. Note that the Hs–Tp pair values used for the power matrix generation do not correspond to real wave measurements. They are obtained following the methodology presented in Section 2.1 and are used to fully characterize the operation of the WEC in the whole additional operational range. The time duration of the simulations to calculate the power production of the WEC has been set to 30 min, as recommended in the International Tower Tank Conference (ITTC) for seakeeping state simulations (Day et al., 2014).

The operation extension associated to a maximum demagnetization (d axis) electrical current of 450 A has been highlighted in blue colour. The whole extension of the power matrices corresponds to the case of a maximum demagnetization electrical current of 550 A. Therefore, it is to be noted that with an increased electrical current capability of the system, the operation of the WEC could be extended to higher significant wave height values H_s, at the expense of a higher economical cost of the electrical system and pending to a mechanical loads analysis that ensures the integrity of the device. Additionally, in line to the results obtained in Sections 3.3.1 and 3.3.2, it is to be observed that a longer extension of the operation of the WEC can be achieved in case of the smaller point absorber (WaveBot) with the same dimensioning of the electrical system.

3.5. Additional energy and hydrogen calculation

Real wave elevation measurements from four far offshore locations (P-00 → {54°N,29.5°W}, P-01 → {48.5°N,39°W}, P-02 → {37.5° N, 57°W}, P-03 → {57°N, 22.5°W}) at the Atlantic ocean and one nearshore location at the Biscay coast (P-04 → {43.37°N, 3.07°W}) (Ulazia et al., 2020) have been used for the calculation of the additional energy/hydrogen generated by the WECs as a result of the extension of their operational range by application of the FW functionality. The wave resource data, downloaded from the *ERA5* dataset (Hersbach et al., 2020), is presented in form of 1 hourly mean values and covers the 2010–2019 time period.

Since solely the additional energy/hydrogen generated by the WECs in case of implementation of the FW strategy is of interest, only the extensions of the power matrices, see Table 4, have been used for the calculations. The results of the additional energy generation of both WECs in the analysed offshore locations are listed in Table 5.

Table 5
Additional energy generation in offshore locations by application of the FW functionality.

Additional energy generation [MWh]						
Device	Max. Current	Location				
		P-00	P-01	P-02	P-03	P-04
WaveBot	450 A	73.98	79.38	25.28	82.99	4
	550 A	117.9	131.67	39.56	127.09	4.75
Flat	450 A	54.82	62.86	20.63	64.85	3.98
	550 A	159.66	177.54	53.44	172.21	6.76

Table 6
Additional hydrogen production in offshore locations by application of the FW functionality.

Additional hydrogen generation [N m^3]						
Device	Max. Current	Location				
		P-00	P-01	P-02	P-03	P-04
WaveBot	450 A	17 614	18 899	6018	19 759	952
	550 A	28 072	31 350	9419	30 259	1131
Flat	450 A	13 053	14 967	4911	15 439	947
	550 A	38 015	42 272	12723	41 002	1609

On account of the difficulties associated to the grid integration in oceanic far offshore locations, the employment of energy vectors such as hydrogen or methanol for the energy storage is supported in those farms. Consequently, the additional hydrogen production of the WECs as a result of the extension of their operational range by application of the FW functionality is presented in Table 6. An energy consumption of 4.2 $^{kWh}/_{N\ m^3}$ (covering all desalination, compression, electrolysis and additional processes) has been used for the computation of the hydrogen production (Serna and Tadeo, 2014).

The results show that important additional energy/hydrogen production could be achieved by extension of the operational range of the WECs with the application of the proposed FW strategy, especially in the far offshore locations. Moreover, it is to be observed that the achievable additional energy/hydrogen gain is more important in WECs with bigger size. For instance, a maximum of 177.54 MWh energy or 42 272 N m^3 hydrogen are to be produced with the Flat WEC at location P-01 during the analysed 20 years. Likewise, a maximum of 131.67 MWh energy or 31 350 N m^3 hydrogen are to be produced by using the WaveBot WEC at the same location. In terms of equivalent production hours, the generated additional energy/hydrogen would correspond to 2270 equivalent production hours of the Flat WEC operating at maximum power and 2095 equivalent production hours of the WaveBot WEC operating at its maximum power.

It is to be observed that the achievable energy/hydrogen gain depends on the dimensioning of the electrical system. If the maximum demagnetization electrical current capability is increased, the actuation of the FW functionality, and therefore the operation of the WEC, can be extended to higher wave significant values H_s and the produced additional energy/hydrogen is also incremented. Moreover, the dimensioning of the electrical system might also affect the selection of the best location for the installation of a WEC. In this way, while the maximum additional energy/hydrogen for a dimensioning of 550 A of demagnetization electrical current is produced at location P-01, the location with maximum additional production is P-03 if the electrical system is dimensioned for 450 A of demagnetization current. Therefore, the wave resource characteristics of a given location might also be important to be considered during the design process of the FW strategy. Finally, with the current control parametrization, the additional energy

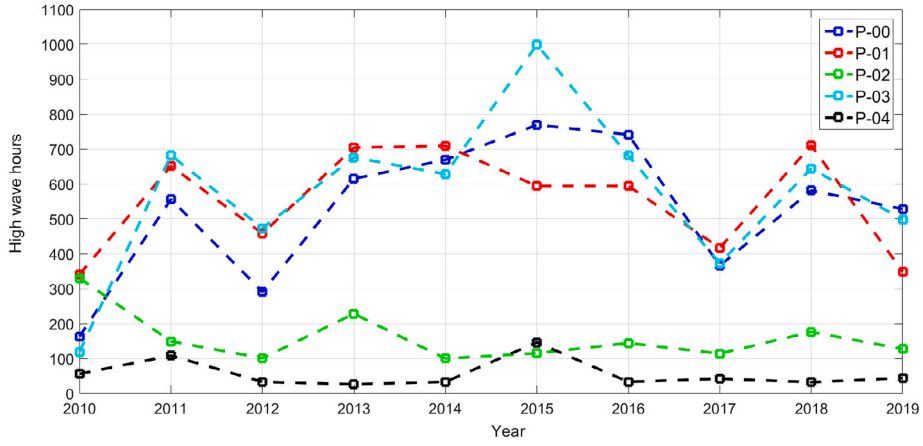

Fig. 11. Yearly evolution of the high wave events (in hours) at the locations analysed in this paper.

production of the WaveBot device is observed to surpass that of the Flat device, when the electrical system is dimensioned for a maximum demagnetization current of 450 A. This fact emphasizes the importance of a multiperspective design procedure of the WECs, adapting their geometry to the characteristics of the sea states and the capabilities of the electrical system.

4. Discussion

The performance of in heave oscillating linear point absorbers has been extensively studied in the literature (Faizal et al., 2014; Bezunartea-Barrio et al., 2020; Piscopo et al., 2018; Rusu, 2018). Essentially, while some works are devoted to the design of the best geometry and size of the point absorbers (Esmaeilzadeh and Alam, 2019), others are aimed to find the optimal control law to be applied to a WEC in order to maximize its power absorption (Babarit and Clément, 2006; Cretel et al., 2011; Coe et al., 2020; Bacelli and Coe, 2020). Regarding the design process of the control strategy, the most recent works in the literature include in their procedures a restriction for the maximum force the PTO system can apply in the point absorber (Coe et al., 2020). However, this restriction is usually treated as a mathematical constraint and its physical origin is neglected. In this analysis, the introduction of a model of the PTO system in the simulations allows to have a fully detailed system and the conversion and treatment of the mathematical restrictions as physical variables, which enables a more detailed design of the whole WEC.

An important aspect to consider during the design process of a WEC is the definition of its operational range, usually limited either by the maximum displacement of the point absorber or the maximum force the PTO system can apply. In the analysis presented in this paper, a FW control algorithm has been proposed and validated as a solution to overcome some restrictions associated to an electrical PTO system based on a PMSLG. As a result of applying the FW functionality, the performance of the PTO system is improved at high velocities of the point absorber, and the operational range of the WEC could be extended to higher significant wave height H_s values. The execution of a similar analysis would result unfeasible if the model of the PTO system would have not been combined with the model of the point absorber, and the electrical limitation had solely been treated as a simple mathematical constraint. The development of advanced optimization problems, which integrate modelling of the physical source of the constraints, is contemplated as a paramount step for the evolution of energy-maximizing strategies applied to WECs.

The benefits of the presented FW functionality have also been found to be related to the size of the WEC. In case of larger WECs, with a higher size, and therefore mass, the implementation of the FW functionality could result especially helpful due to their prolonged malfunction after a sea state of high excitation, consequence of the high inertia associated to their mass. Hence, the FW strategy could result in important improvements of the operation of the WEC during longer periods of time. A detailed analysis of the sensitivity of the energy gain associated to the FW functionality with respect to the PTO control strategy/parametrization is also considered as an important future work.

The benefits of the presented FW functionality could also be linked to the characteristics of the wave resource at the installation site of a WEC, see Fig. 11. The results presented in the analysis have shown that the actuation of the proposed functionality enables operation of the device at sea states with high wave amplitude. Consequently, while at locations with low wave heights the application of the FW strategy could not result remarkably helpful, the potential benefit of its implementation at locations with high wave heights is evident. Therefore, in this case, the implementation of the FW functionality would result more beneficial at the far offshore locations P-00, P-01 and P-03, where the amount of hours with high waves is larger than at locations P-02 and P-O4. Meteorological analyses of the wave characteristics at a defined location prior to the installation of the device could help determine the suitability of the strategy to be or not be implemented in the WEC.

Finally, the industrial application of the strategy is considered to be significantly easier than complex optimization algorithms that could be problematic when being implemented and executed in real time applications in a microprocessor based CCU (Converter Control Unit). In fact, the proposed functionality could be considered as a plug-&-play element of an extensively industrially mature control algorithm, as it is the FOC strategy. The economical benefits associated to the installation of the FW strategy could be measured by the additional energy/hydrogen production achieved as a result of the extension of the operation of the WEC. It must be taken into account that the application of the FW strategy requires an overdimensioning of the electrical system, which will result in an increment of its economical cost and will have to be considered when studying the economical viability of the project.

5. Conclusions

A FW control functionality to improve and extend the operation of linear in heave oscillating point absorber based WECs has been proposed in this paper. The PTO system associated to the linear point absorbers is electrical, based on a PMSLG. As a result of the conducted analysis, the potential benefits of implementing this functionality on the energy/hydrogen generation of two different sized WECs has been stressed.

The implementation of a FW strategy has been found to effectively reduce the magnetic flux of the stator of the electrical generator during

sea states of high excitation, i.e., sea states that cause high velocity motions of the point absorber. The application of the FW functionality during those periods enables to keep an adequate tracking of the reference PTO force and to avoid overcurrents that may damage the electrical system. In fact, by injecting electrical current in a controlled way, the performance of the electrical PTO system is remarkably improved and its safety ensured, which allows to extend the operation of the WEC to higher values of the significant wave height H_s; always subject to a mechanical loads analysis that ensures the integrity of the device in such high wave conditions.

The effect of the proposed FW strategy has also been found to be dependent on the size, and therefore, hydrodynamic characteristics of the point absorber of the WEC. The application of the FW strategy has been found to be more necessary for larger WECs, in which the recovery from a problematic sea state is worse due to the bigger inertia. In case of smaller WECs, their operational range could be further extended with the same dimensioning of the electrical system, always subject to the control parametrization.

Finally, the additional energy/hydrogen production of both different sized WECs have been computed using real wave resource data in four far offshore locations in the Atlantic ocean and one nearshore location in the Biscay coast. The obtained results show that important additional energy/hydrogen could be produced as a result of the extension of the operation of the point absorber using the FW functionality. These economical benefits, in combination with the overdimensioning of the electrical system due to the proposed FW functionality, should be considered when assessing the economic viability of the installation of the WEC.

CRediT authorship contribution statement

Aitor Saenz-Aguirre: Conceptualization, Methodology, Software, Writing – original draft, Writing – review & editing. **Alain Ulazia:** Conceptualization, Writing – original draft, Writing – review & editing. **Gabriel Ibarra-Berastegui:** Investigation, Supervision, Writing – review & editing. **Jon Saenz:** Supervision, Writing – review & editing.

Declaration of competing interest

The authors declare that they have no known competing financial interests or personal relationships that could have appeared to influence the work reported in this paper.

Acknowledgements

Authors acknowledge financial support by the Spanish Ministry of Science and Innovation, Agencia Española de Investigación (grant PID2020-116153RB-I00/AEI/10.13039/501100011033) and the University of the Basque Country under the contract (UPV/EHU, GIU20/008).

References

Ammar, R., Trabelsi, M., Mimouni, M.F., Ahmed, H.B., Benbouzid, M., 2017. Flux weakening control of PMSG based on direct wave energy converter systems. In: 2017 International Conference on Green Energy Conversion Systems (GECS). IEEE, pp. 1–7.

António, F.d.O., 2008. Phase control through load control of oscillating-body wave energy converters with hydraulic PTO system. Ocean Eng. 35 (3–4), 358–366.

Arinaga, R.A., Cheung, K.F., 2012. Atlas of global wave energy from 10 years of reanalysis and hindcast data. Renew. Energy 39 (1), 49–64.

Babarit, A., 2015. A database of capture width ratio of wave energy converters. Renew. Energy 80, 610–628. http://dx.doi.org/10.1016/j.renene.2015.02.049.

Babarit, A., Clément, A., 2006. Optimal latching control of a wave energy device in regular and irregular waves. Appl. Ocean Res. 28 (2), 77–91. http://dx.doi.org/10.1016/j.apor.2006.05.002, URL http://www.sciencedirect.com/science/article/pii/S0141118706000423.

Babarit, A., Delhommeau, G., 2015. Theoretical and numerical aspects of the open source BEM solver NEMOH.

Bacelli, G., Coe, R.G., 2020. Comments on control of wave energy converters. IEEE Trans. Control Syst. Technol..

Bezunartea-Barrio, A., Fernandez-Ruano, S., Maron-Loureiro, A., Molinelli-Fernandez, E., Moreno-Buron, F., Oria-Escudero, J., Rios-Tubio, J., Soriano-Gomez, C., Valea-Peces, A., Lopez-Pavon, C., et al., 2020. Scale effects on heave plates for semi-submersible floating offshore wind turbines: case study with a solid plain plate. J. Offshore Mech. Arct. Eng. 142 (3).

Borgarino, B., Babarit, A., Ferrant, P., 2012. Impact of wave interactions effects on energy absorption in large arrays of wave energy converters. Ocean Eng. 47, 79–88.

Brekken, T.K.A., 2011. On model predictive control for a point absorber wave energy converter. In: 2011 IEEE Trondheim PowerTech. pp. 1–8.

Calado, M., Godinho, P., Mariano, S., 2012. Design of a new linear generator for wave energy conversion based on analytical and numerical analyses. J. Renew. Sustain. Energy 4 (3), 033117.

Cargo, C.J., Plummer, A.R., Hillis, A.J., Schlotter, M., 2012. Determination of optimal parameters for a hydraulic power take-off unit of a wave energy converter in regular waves. Proc. Inst. Mech. Eng. A 226 (1), 98–111.

Child, B., Venugopal, V., 2010. Optimal configurations of wave energy device arrays. Ocean Eng. 37 (16), 1402–1417.

Coe, R.G., Bacelli, G., Olson, S., Neary, V.S., Topper, M.B., 2020. Initial conceptual demonstration of control co-design for WEC optimization. J. Ocean Eng. Mar. Energy 1–9.

Coe, R., Bacelli, G., Patterson, D., Wilson, D., Advanced WEC dynamics & controls FY16 testing report; SAND report: SAND2016-10094.

Cretel, J.A., Lightbody, G., Thomas, G.P., Lewis, A.W., 2011. Maximisation of energy capture by a wave-energy point absorber using model predictive control. IFAC Proc. Vol. 44 (1), 3714–3721.

Cummins, W., 1962. The impulse response function and ship motion. Schiffstechnik (9), 101–109.

Danielsson, O., 2006. Wave Energy Conversion: Linear Synchronous Permanent Magnet Generator (Ph.D. thesis). Acta Universitatis Upsaliensis.

Day, S., Penesis, I., Babarit, A., Fontaine, A., He, Y., Kraskowski, M., Murai, M., Salvatore, F., Shin, H., et al., 2014. Ittc recommended guidelines: Wave energy converter model test experiments (7.5-02-07-03.7). In: 27th International Towing Tank Conference. pp. 1–13.

Edwards, K., Mekhiche, M., et al., 2014. Ocean power technologies powerbuoy®: system-level design, development and validation methodology. In: Proceedings of the 2nd Marine Energy Technology Symposium. METS2014.

Esmaeilzadeh, S., Alam, M.R., 2019. Shape optimization of wave energy converters for broadband directional incident waves. Ocean Eng. 174 (December 2018), 186–200. http://dx.doi.org/10.1016/j.oceaneng.2019.01.029.

Faedo, N., Peña-Sanchez, Y., Ringwood, J.V., 2018. Finite-order hydrodynamic model determination for wave energy applications using moment-matching. Ocean Eng. 163, 251–263.

Faizal, M., Ahmed, M.R., Lee, Y.-H., 2014. A design outline for floating point absorber wave energy converters. Adv. Mech. Eng. 6, 846097.

Falcao, A.d.O., 2010. Wave energy utilization: A review of the technologies. Renew. Sustain. Energy Rev. 14 (3), 899–918.

Falcão, A.F.d.O., 2010. Wave energy utilization: A review of the technologies. Renew. Sustain. Energy Rev. 14 (3), 899–918. http://dx.doi.org/10.1016/j.rser.2009.11.003, URL http://www.sciencedirect.com/science/article/pii/S1364032109002652.

Falnes, J., 1999. Wave-energy conversion through relative motion between two single-mode oscillating bodies.

Gaeta, M.G., Segurini, G., Moreno, A.M., Archetti, R., 2020. Implementation and validation of a potential model for a moored floating cylinder under waves. J. Mar. Sci. Eng. 8 (2), 131.

Garcia-Teruel, A., DuPont, B., Forehand, D.I., 2020. Hull geometry optimisation of wave energy converters: On the choice of the optimisation algorithm and the geometry definition. Appl. Energy 280, 115952.

García-Violini, D., Faedo, N., Jaramillo-Lopez, F., Ringwood, J.V., 2020. Simple controllers for wave energy devices compared. J. Mar. Sci. Eng. 8 (10), 793.

Genest, R., Ringwood, J.V., 2016. A critical comparison of model-predictive and pseudospectral control for wave energy devices. J. Ocean Eng. Mar. Energy 2 (4), 485–499.

Giorgi, G., Gomes, R.P., Henriques, J.C., Gato, L.M., Bracco, G., Mattiazzo, G., 2020. Detecting parametric resonance in a floating oscillating water column device for wave energy conversion: Numerical simulations and validation with physical model tests. Appl. Energy 276, 115421.

Giorgi, G., Penalba, M., Ringwood, J., 2016. Nonlinear hydrodynamic models for heaving buoy wave energy converters.

Hansen, R.H., Kramer, M.M., Vidal, E., 2013. Discrete displacement hydraulic power take-off system for the wavestar wave energy converter. Energies 6 (8), 4001–4044.

Hasselmann, K., Barnett, T., Bouws, E., Carlson, H., Cartwright, D., Enke, K., Ewing, J., Gienapp, H., Hasselmann, D., Kruseman, P., et al., 1973. Measurements of wind-wave growth and swell decay during the Joint North Sea Wave Project (JONSWAP). Ergänzungsheft 8–12.

Hersbach, H., Bell, B., Berrisford, P., Hirahara, S., Horányi, A., Muñoz-Sabater, J., Nicolas, J., Peubey, C., Radu, R., Schepers, D., Simmons, A., Soci, C., Abdalla, S., Abellan, X., Balsamo, G., Bechtold, P., Biavati, G., Bidlot, J., Bonavita, M., De Chiara, G., Dahlgren, P., Dee, D., Diamantakis, M., Dragani, R., Flemming, J., Forbes, R., Fuentes, M., Geer, A., Haimberger, L., Healy, S., Hogan, R.J., Hólm, E., Janisková, M., Keeley, S., Laloyaux, P., Lopez, P., Lupu, C., Radnoti, G., de Rosnay, P., Rozum, I., Vamborg, F., Villaume, S., Thépaut, J.-N., The ERA5 global reanalysis. Q. J. R. Meteorol. Soc. n/a (n/a). http://dx.doi.org/10.1002/qj.3803.

Isaacson, M., Mathai, T., Mihelcic, C., 1990. Hydrodynamic coefficients of a vertical circular cylinder. Can. J. Civil Eng. 17 (3), 302–310.

Ivanova, I.A., Agren, O., Bernhoff, H., Leijon, M., 2005. Simulation of wave-energy converter with octagonal linear generator. IEEE J. Ocean. Eng. 30 (3), 619–629.

Jonkman, J.M., Robertson, A.N., Hayman, G.J., 2015. HydroDyn User's Guide and Theory Manual. NREL.

Kassem, A.M., Besheer, A.H., Atawi, I.E., 2015. Kalmen estimator as a robust solution for output power maximization of wave energy converter. IEEJ Trans. Electr. Electron. Eng. 10 (4), 390–395.

Korde, U.A., 2003. Systems of reactively loaded coupled oscillating bodies in wave energy conversion. Appl. Ocean Res. 25 (2), 79–91.

LHEEA Centrale Nantes, 2019. NREL NWTC FAST version 8. Available online: https://nwtc.nrel.gov/fast8/ (accessed on 10 oct 2019).

Lu, D., Kar, N.C., 2010. A review of flux-weakening control in permanent magnet synchronous machines. In: 2010 IEEE Vehicle Power and Propulsion Conference. IEEE, pp. 1–6.

Ma, J.D., Wu, B., Zargari, N.R., Rizzo, S.C., 2001. A space vector modulated CSI-based AC drive for multimotor applications. IEEE Trans. Power Electron. 16 (4), 535–544.

Mayo, A.P., Saenz-Aguirre, A., Martín, F., Vadillo, J., 2020. FOC-droop control strategy for PMSM fed paralleled multi-inverter power systems oriented to aeronautical applications. Electr. Power Syst. Res. 185, 106369.

Neary, V.S., Ahn, S., Seng, B.E., Allahdadi, M.N., Wang, T., Yang, Z., He, R., 2020. Characterization of extreme wave conditions for wave energy converter design and project risk assessment. J. Mar. Sci. Eng. 8 (4), 289.

NREL NWTC, 2020. http://130.66.47.2/cgi-bin/hgweb.cgi/nemoh/ (accessed on 3 nov 2020).

Park, R.H., 1929. Two-reaction theory of synchronous machines generalized method of analysis-part I. Trans. Am. Inst. Electr. Eng. 48 (3), 716–727.

Penalba, M., Ringwood, J.V., 2019. Linearisation-based nonlinearity measures for wave-to-wire models in wave energy. Ocean Eng. 171, 496–504.

Penalba, M., Ringwood, J.V., 2020. Systematic complexity reduction of wave-to-wire models for wave energy system design. Ocean Eng..

Pierson, Jr., W.J., Moskowitz, L., 1964. A proposed spectral form for fully developed wind seas based on the similarity theory of SA Kitaigorodskii. J. Geophys. Res. 69 (24), 5181–5190.

Piscopo, V., Benassai, G., Della Morte, R., Scamardella, A., 2018. Cost-based design and selection of point absorber devices for the mediterranean sea. Energies 11 (4), 946.

Polinder, H., Damen, M.E., Gardner, F., 2004. Linear PM generator system for wave energy conversion in the AWS. IEEE Trans. Energy Convers. 19 (3), 583–589.

Prudell, J., Stoddard, M., Amon, E., Brekken, T.K.A., von Jouanne, A., 2010. A permanent-magnet tubular linear generator for ocean wave energy conversion. IEEE Trans. Ind. Appl. 46 (6), 2392–2400.

Ramirez, D., Mendonça, H., Blanco, M., Martinez, F., 2019. Non-linear vector current source for the control of permanent magnet synchronous generators in wave energy applications. IET Renew. Power Gener. 13 (13), 2409–2417.

Ruehl, K., 2011. Time-Domain Modeling of Heaving Point Absorber Wave Energy Converters, Including Power Take-Off and Mooring (Master Thesis). Mechanical Engineering Department, Oregon State University.

Rusch, C.J., Mundon, T.R., Maurer, B.D., Polagye, B.L., 2020. Hydrodynamics of an asymmetric heave plate for a point absorber wave energy converter. Ocean Eng. 215, 107915.

Rusu, E., 2018. Numerical modeling of the wave energy propagation in the Iberian nearshore. Energies 11 (4), 980.

Rusu, E., Onea, F., 2016. Estimation of the wave energy conversion efficiency in the Atlantic Ocean close to the European islands. Renew. Energy 85, 687–703.

Rusu, E., Onea, F., 2018. A review of the technologies for wave energy extraction. Clean Energy 2 (1), 10–19.

Sergiienko, N., Cazzolato, B., Ding, B., Hardy, P., Arjomandi, M., 2017. Performance comparison of the floating and fully submerged quasi-point absorber wave energy converters. Renew. Energy 108, 425–437.

Serna, A., Tadeo, F., 2014. Offshore hydrogen production from wave energy. Int. J. Hydrogen Energy 39 (3), 1549–1557.

Sirigu, S.A., Foglietta, L., Giorgi, G., Bonfanti, M., Cervelli, G., Bracco, G., Mattiazzo, G., 2020. Techno-economic optimisation for a wave energy converter via genetic algorithm. J. Mar. Sci. Eng. 8 (7), 482.

Sullivan, A.C., Lightbody, G., 2016. Predictive control of a wave to wire energy conversion system—The importance of field weakening. In: 2016 UKACC 11th International Conference on Control (CONTROL). IEEE, pp. 1–6.

Tursini, M., Chiricozzi, E., Petrella, R., 2009. Feedforward flux-weakening control of surface-mounted permanent-magnet synchronous motors accounting for resistive voltage drop. IEEE Trans. Ind. Electron. 57 (1), 440–448.

Ulazia, A., Esnaola, G., Serras, P., Penalba, M., 2020. On the impact of long-term wave trends on the geometry optimisation of oscillating water column wave energy converters. Energy 206, 118146.

Vantorre, M., Banasiak, R., Verhoeven, R., 2004. Modelling of hydraulic performance and wave energy extraction by a point absorber in heave. Appl. Ocean Res. 26 (1–2), 61–72.

Wang, Z., Chen, J., Cheng, M., Chau, K., 2015. Field-oriented control and direct torque control for paralleled VSIs fed PMSM drives with variable switching frequencies. IEEE Trans. Power Electron. 31 (3), 2417–2428.

Wang, L., Kolios, A., Cui, L., Sheng, Q., 2018. Flexible multibody dynamics modelling of point-absorber wave energy converters. Renew. Energy 127, 790–801.

Xu, L., Ye, L., Zhen, L., El-Antably, A., 1995. A new design concept of permanent magnet machine for flux weakening operation. IEEE Trans. Ind. Appl. 31 (2), 373–378.

Zhao, C., Thies, P.R., Ye, Q., Lars, J., 2020. System integration and coupled effects of an OWT/WEC device. Ocean Eng. 108405.